Gas Dynamics in the LINER Galaxy NGC 5005: Episodic Fueling of a Nuclear Disk

Kazushi Sakamoto[1,2,3], Andrew J. Baker[1], and Nick Z. Scoville[1]

ABSTRACT

We report high-resolution CO(1–0) observations in the central 6 kpc ($1'$) of the LINER galaxy NGC 5005 with the Owens Valley Radio Observatory millimeter array. Molecular gas is distributed in three components — a ring at a radius of about 3 kpc, a strong central condensation, and a stream to the northwest of the nucleus but inside the 3 kpc ring. The ring shows systematic noncircular motions, with apparent inward velocities of ~ 50 km s^{-1} on the minor axis. The central condensation is a disk of ~ 1 kpc radius with a central depression of ~ 50 pc radius. This disk has a molecular gas mass of $\sim 2 \times 10^9$ $M_\odot$; it shows a steep velocity gradient and a velocity range (~ 750 km s^{-1}) 30% larger than the velocity width of the rest of the galaxy. The stream between the 3 kpc ring and the nuclear disk lies on a straight dust lane seen in the optical. If this material moves in the plane of the galaxy, it lies at a radius of ~ 1 kpc but has a velocity offset by up to ~ 150 km s^{-1} from galactic rotation. We suggest that an optically inconspicuous stellar bar lying within the 3 kpc ring can explain the observed gas dynamics. This bar is expected to connect the nuclear disk and the ring along the position angle of the northwest stream. A position-velocity cut in this direction reveals features which match the characteristic motions of gas in a barred potential. Our model indicates that gas in the northwest stream is on an x_1 orbit at the bar's leading edge; it is falling into the nucleus with a large noncircular velocity, and will eventually contribute $\sim 2 \times 10^8$ $M_\odot$ to the nuclear disk. If most of this material merges with the disk on its first passage of pericenter, the gas accretion rate during the collision will be ~ 50 $M_\odot$ yr^{-1}. We associate the disk with an inner 2:1 Lindblad resonance and attribute its large linewidth to favorably oriented elliptical orbits rather than (necessarily) to a large central mass. The 3 kpc ring is likely an inner 4:1 Lindblad resonance ring — or a pair of tightly wound spiral arms — arising at the bar ends. Both scenarios can explain the apparent noncircular motions in the ring. The high rate of bar-driven inflow and the irregular appearance of the northwest stream suggest that a major fueling event is in progress in NGC 5005. Such episodic (rather than continuous) gas supply can regulate the triggering of starburst and accretion activity in galactic nuclei.

Subject headings: galaxies: dynamics and kinematics — galaxies: ISM — galaxies: spiral — galaxies: active — galaxies: starburst

---

[1]Owens Valley Radio Observatory, Caltech 105-24, Pasadena, CA 91125

[2]Nobeyama Radio Observatory, Minamisaku, Nagano, 384-1305, Japan; E-mail(KS): sakamoto@nro.nao.ac.jp

[3]Guest investigator of the RGO Astronomy Data Center

1. Introduction

NGC 5005 is an Sbc galaxy hosting a low ionization nuclear emission-line region (LINER) at its center (Keel 1983). We list some of the system's global properties in Table 1. Ho *et al.* (1997) propose that the nucleus is accretion-powered, on the basis of a broad (1650 km s^{-1} FWHM) component in a fit to the nuclear Hα line. Risaliti *et al.* (1999) suggest on the basis of X-ray observations that the active nucleus is fully obscured by an absorbing column of $N_H > 10^{24}$ cm^{-2}. An alternative driver of nuclear emission may be ongoing OB star formation which follows a starburst $\sim 10^9$ yr ago (Goodrich & Keel 1986). On larger scales, NGC 5005 is classed as SAB (moderately barred) by de Vaucouleurs *et al.* (1991), although the location of the bar-like distortion is not apparent in optical images. The galaxy is thought to comprise a binary pair with NGC 5033, a spiral of similar size and redshift at a projected separation of ~ 250 kpc (for $d = 21.3$ Mpc: Tully 1988). Neither galaxy displays distortions to its optical morphology, suggesting that there has been no significant recent interaction.

— Table 1 —

We first observed the molecular gas in NGC 5005 in the course of a survey of 20 nearby spirals (Sakamoto *et al.* 1999a), using the Owens Valley Radio Observatory (OVRO) millimeter array. We found a strong concentration of molecular gas ($\sim 10^9 M_\odot$) in the central kpc and an [apparently] incomplete ring of gas at a radius of 3 kpc. The nucleus revealed a very steep velocity gradient in CO — $\Delta V \sim 700$ km s^{-1} within $10''$ or $\Delta V/\Delta r \gtrsim 800$ km s^{-1} kpc^{-1} — consistent with optical observations (Filippenko & Sargent 1985). The combination of the massive nuclear gas concentration, the large central velocity gradient, and the nearly circular ring motivated a more detailed study of this galaxy's gas dynamics and their implications for nuclear fueling. Our original observations had relatively low sensitivity and resolution: the $5'' \times 4''$ (0.5 kpc) beam only marginally resolved the ~ 1 kpc structure in the nucleus. In this paper, we report high-resolution and high-sensitivity CO(1–0) observations of NGC 5005 using data from three configurations of the OVRO array. These observations include data from the new U configuration, which with baselines ~ 400 m permits $\sim 1''$ resolution at this wavelength.

2. Observational Data

2.1. OVRO CO(1–0) observations

Our new aperture synthesis observations of the CO(1–0) emission in NGC 5005 were taken with the OVRO millimeter array between February and May 1998, for a single pointing center at $\alpha_{1950} = 13^{\rm h}08^{\rm m}37\overset{\rm s}{.}7$ and $\delta_{1950} = +37°19'29''\!.0$. The array consists of six 10.4 m telescopes equipped with SIS receivers. Digital correlators were configured to cover 336 MHz (874 km s^{-1}) with 4 MHz (10.4 km s^{-1}) resolution. Analog correlators recorded 1 GHz continuum data from the signal and image bands. For gain calibration, we observed the quasar 1308+326 every half-hour; 3C273 was observed for passband calibration. The chopper-wheel method was used to correct for the atmospheric transmission. An absolute flux scale (uncertain to $\sim 15\%$) was established by comparing the apparent strengths of 1308+326 and Uranus. We adopt 1.5 Jy as the flux density for 1308+326 in the spring of 1998, an increase over the 1.0 Jy estimated for the original [survey] data from April 1997. Our observations were obtained in the L, H, and [new] U configurations; when combined with the preliminary data, we had the equivalent of five full transits with projected baselines from 10.4 m to 400 m. The visibility data were calibrated with the OVRO MMA software (Scoville *et al.* 1993) and mapped with the NRAO AIPS package.

Three combinations of configuration and weighting were used to make maps (Table 2), to which we will refer according to their low ($4''$), medium ($2''\!.7$), and high ($1''\!.5$) resolutions. Figure 1 presents all three sets of zeroth and first moment maps, while Figure 2 shows the low-resolution channel maps. The fraction of the total flux recovered by each of our maps is estimated from comparisons of our data with single-dish observations from the FCRAO 14 m and the IRAM 30 m telescopes (Young *et al.* 1995; Braine *et al.* 1993). Each data cube was corrected for the primary beam response of the OVRO antennas (a Gaussian with HPBW = $60''$), convolved with the single-dish beam ($45''$ for FCRAO and $23''$ for IRAM), and sampled at the pointing centers of the single-dish observations to obtain values comparable to the single-dish fluxes. Our low and medium-resolution maps recover about 74% of the total flux in the central $45''$ and 93% in the central $23''$. The high-resolution map recovers 50% of the total flux in $45''$ but 75% in the central $23''$, where there is a strong concentration of molecular gas. We made no correction to our data for missing flux. We

did correct for primary beam attenuation before measuring flux from our maps, although this correction was not applied to the maps shown in the figures.

— Table 2 —

— Figures 1 – 2 —

2.2. Supplementary data

For comparison purposes, we have obtained data for NGC 5005 at several other wavelengths from archives and the literature. Figure 3 shows a Strömgren y band ($\lambda = 550$ nm, $\Delta\lambda = 20$ nm) image obtained with the 2.5 m Isaac Newton Telescope at the Observatorio del Roque de los Muchachos, Spain. Dust lanes in this image trace the spiral arms, which if trailing imply (since the east side of the galaxy is receding) that the northwest half of the galaxy is nearer to us.

— Figure 3 —

Figure 4 shows a WFPC2 image obtained with the Hubble Space Telescope (HST).[4] This image was taken in the F547M filter ($\lambda = 547$ nm, $\Delta\lambda = 49$ nm). Cosmic ray hits were removed and images from the four chips of the camera were combined with IRAF and STSDAS. The absolute position of the HST image relies on the HST Guide Star Catalog and is accurate to about $0\rlap{.}''5$. The sharpness of the dust lane to the northwest of the nucleus supports the view that this side of the galaxy is nearer, and that the spiral arms are trailing.

— Figure 4 —

NGC 5005 has been observed with the VLA on several occasions. A compact central source is only marginally resolved at $\sim 1''$ resolution. Table 3 lists the measurements of the position of the central source. We also present the mean position of the radio source, which coincides well with the dynamical center determined from our CO data (§3.1).

— Table 3 —

3. Results

Our CO maps show an oval ring of $\sim 1'$ diameter and a strong central condensation, confirming our previous observations (Sakamoto *et al.* 1999a). In addition to these two structures, we find a "northwest

stream" between the ring and the central peak with unusually large noncircular velocities. We describe each of these three components in order of increasing radius.

3.1. The nuclear disk

The medium and high-resolution maps of Figure 1 now clearly resolve the nuclear gas disk. The disk has an extent of $20'' \times 10''$ in the medium-resolution map, elongated along the isophotal major axis of the galaxy (p.a. $= 65°$) as determined on large scales. Its extent is smaller in the high-resolution map, probably because of lower flux recovery and lower surface-brightness sensitivity. The emission feature $\sim 6''$ northwest of the nucleus is kinematically distinct from the nuclear disk; we discuss it in the next section. The total CO flux of the nuclear disk is $S_{\mathrm{CO}} = 310$ Jy km s^{-1}, which corresponds to $M_{\mathrm{gas}} = 2.3 \times 10^9$ for the Galactic conversion factor $N_{\mathrm{H_2}}/I_{\mathrm{CO}} = 3 \times 10^{20}$ cm^{-2} (K km s^{-1})$^{-1}$ (Scoville *et al.* 1987; Solomon *et al.* 1987; Strong *et al.* 1988) and a factor of 1.36 for heavy elements.

We fit the velocity field in the nucleus to a tilted ring model using the AIPS task GAL. The high-resolution data were used for the model input; the derived kinematic parameters are listed in Table 4. The inclination and major-axis position angle of the nuclear disk agree well with those from fits to the isophotes of the galaxy as a whole (see Table 1). The slight differences (less than $10°$ for both position angle and inclination) may be due to noncircular motions in the nuclear disk, a warp of the galactic disk, an incorrect assumption for the intrinsic axial ratio in the isophote fit, or statistical errors in both measurements. We will adopt the large-scale isophotal values for inclination and position angle in the rest of our analysis. The inferred dynamical center coincides within $0\rlap{.}''5$ with the mean position of the nuclear radio source in Table 3. The CO emission is largely axisymmetric about the dynamical center, with a slight ($\sim 1''$ or 100 pc) shift of the emission centroid to the northeast.

— Table 4 —

In the high-resolution map, CO(1–0) emission weakens at the dynamical center, due to absence of gas or higher excitation at the nucleus. The S-shaped contours in the isovelocity map near systemic velocity indicate noncircular motions in the nuclear disk. The noncircular component of the velocity is directed out-

---

ward on the disk's minor axis. The full range of velocities in the nuclear disk (in the medium-resolution data) is 740 km s^{-1}, or 830 km s^{-1} if corrected for the inclination of 62°. This is about 30% wider than the HI line width of the galaxy, $W_{\rm HI} = 556$ km s^{-1} (not corrected for inclination: de Vaucouleurs *et al.* 1991), as has been noticed previously (Braine *et al.* 1993). The large linewidth is confined to the nuclear disk, as seen from a position-velocity cut along its major axis (Figure 5). The dynamical mass and the mass fraction of gas within radii of 5″ (0.5 kpc) and 30″ (3.1 kpc) are given in Table 5. The total mass in the central kpc (2×10^{10} $M_\odot$, derived assuming circular rotation) almost certainly overestimates the true dynamical mass, as we will discuss in §4.1; but this estimate imposes an upper limit on any large mass concentration in the galactic center. Figure 6 shows that the nuclear CO emission coincides with a dark arc (on the near side of the galaxy) in the optical. The center of the nuclear disk falls on a conical optical feature whose wide opening angle ($\sim 120°$) may be consistent with outflow out of the galactic plane.

— Figure 5 —

— Table 5 —

— Figure 6 —

3.2. The northwest stream

The emission from the northwest stream between the nuclear disk and the 3 kpc ring has anomalously high velocities which are most easily seen in channel maps. In Figure 2, strong emission is seen 5″ – 10″ northwest of the galactic center in at least the velocity channels from $938 – 1062$ km s^{-1} (if not more). The same structure is seen with better spatial and velocity resolutions in the medium-resolution channel maps (Figure 7), most clearly from $979 – 1083$ km s^{-1}. The emission is anomalous in that *it is redshifted with respect to the systemic velocity although it appears on the eastern, approaching side of the galaxy.* The (line-of-sight) velocity offset between this stream and the galaxy rotation estimated from emission elsewhere is as large as ~ 150 km s^{-1}. This feature is definitely real: it is seen in multiple subsets of our data at the same location and velocity. If it traces material moving radially in the galactic plane, the implied motion is at 200 km s^{-1} (about half the free-fall velocity) directed *inward.*

— Figure 7 —

The size of the northwest stream in the high-resolution map is 5″ × 3″ (0.5 × 0.3 kpc), with its major axis running in an east-west direction. Due to missing flux, this map may underestimate the feature's true extent — possibly closer to ~ 1 kpc as seen in the medium-resolution map. The CO flux (in the medium-resolution map) and the CO-derived mass of molecular gas are $S_{\rm CO} = 20$ Jy km s^{-1} and $M_{\rm gas} = 1.5 \times 10^8$ $M_\odot$ respectively. The centroid of the component is at ~ 6 ″ northwest (p.a. = −70°) of the dynamical center. The galactocentric radius of this centroid is 1.0 kpc if the stream is moving in the galactic plane. The velocity gradient in the stream also runs from east to west with higher velocities to the east; the total linewidth is roughly 100 km s^{-1}. Figure 4 reveals that the northwest stream coincides with a dust lane observed optically. This lane lies to the west of the nucleus and runs from the nuclear disk in the east to the 3 kpc ring in the west. The molecular gas of the northwest stream falls in the middle of the dust lane, where there is a dark feature in the optical image.

3.3. The 3 kpc ring

The low-resolution maps (Figures 1 and 2) show a CO ring at a radius of $\sim 30″$ (3 kpc) as in our previous observations. In these maps, the 3 kpc ring is now found to be nearly continuous, completely encircling the center with few gaps. The ring is nearly circular when deprojected, as seen from comparing it to the reference ellipse (an appropriately projected circle) in the maps. Most of the ring emission lies within the annulus from $20″ – 40″$ ($2 – 4$ kpc), although the outer boundary is uncertain because of the primary beam attenuation. The total mass of molecular gas in this annulus is 2.2×10^9 $M_\odot$. The mean and peak surface densities in this region are $\langle \Sigma_{\rm gas} \rangle = 40$ $M_\odot$ pc^{-2} and $\Sigma_{\rm gas}^{\rm peak} = 200$ $M_\odot$ pc^{-2} respectively, after correction for inclination.

The kinematics of the ring seen in the channel maps (Figure 2) are intriguing. Emission in each channel is *not* reflection-symmetric about the major axis of the galaxy (i.e. the major axis of the ellipse). The asymmetry is such that the emission on the far/near (i.e. SE/NW) side of the galaxy is consistently shifted towards the receding/approaching (i.e. to the NE/SW) side of the minor axis. This is most obviously seen at systemic velocity in the 938 km s^{-1} channel. The emission centroids from the ring and the nucleus are indeed aligned, but the alignment differs by 30° from the galaxy's minor axis. Attributing

this offset to an error in the position angle determined from the galaxy's outer isophotes is unwise: it is hard to make an error as large as 30° given the large inclination and undisturbed morphology.[5] The adopted isophotal position angle is also supported by the fact that the highest and lowest-velocity emission from the ring appears on the galaxy's major axis (see the 658, 689, and 1218 km s^{-1} channels in Figure 2). The kinematic major axis of the nuclear disk has p.a. $\approx$ 70°, also in close agreement with the isophotal major axis. We instead ascribe the asymmetries in the channel maps to systematic noncircular motions in the ring. On the minor axis, these motions appear inward, since the emission on the far/near side has lower/higher velocity than systemic. The consistency of the asymmetries from channel to channel suggests that the noncircular motion is systematic and exists across the ring, although it is not observable near the major axis.

In optical images (Figures 3 and 4), the ring appears as a dark arc on the near side of the galaxy. A dark spiral lane clearly emerges from this part of the ring and winds to the southwest at larger radius. A counterpart to this spiral feature on the far side of the galaxy would be harder to see, but there are hints of optically bright patches emanating from the ring to the northeast. We do not detect CO emission from the spiral arms located outside the ring.

4. Gas dynamics in NGC 5005

The contrast in surface density between the nuclear molecular disk and the surrounding region within the 3 kpc ring is striking; it is also similar to the gas morphology often seen in the nuclei of barred galaxies (Sakamoto *et al.* 1999a). Beyond its appearance, the degree of central concentration in this galaxy is (numerically) one of the highest in the Sakamoto *et al.* (1999b) survey, whose results show that barred galaxies in general have higher degrees of gas concentration than their unbarred counterparts. We propose that NGC 5005 contains a small bar within its 3 kpc ring, which builds up the central gas condensation and is itself traced by the northwest stream. We locate this bar in a roughly east-west direction so that the northwest stream can be produced by a shock along the dust lane at its leading edge. The central depression in the nuclear disk may result from concentration of

gas towards x_2 orbits at the inner 2:1 Lindblad resonance of the bar, although it may also reflect outflow or a variation in excitation. The 3 kpc ring likely arises at the end of the bar, due to gas accumulation in either an inner 4:1 Lindblad resonance region or a pair of tightly wound spiral arms. A schematic view of our interpretation is shown in Figure 8. We present below our detailed cases for the existence of the bar[6] and the origin of the 3 kpc ring, along with a brief discussion of the role played by these structures in fueling the nucleus.

— Figure 8 —

4.1. Bar-driven gas dynamics

Figure 9 shows a position-velocity cut at a position angle of 80°, roughly along the hypothesized bar. The cut is 5″ wide and therefore includes the emission from the northwest stream. The p-v diagram shows two distinct kinematic components. The component with the steeper velocity gradient arises in the nuclear disk; the component with the shallower gradient originates in the northwest stream [at $(+5'', +100$ km s$^{-1})$] and parts of the 3 kpc ring. The overall "tilted X" pattern is characteristic of p-v diagrams in models of bar-driven gas dynamics: each kinematic component corresponds to a major family of noncircular orbits supported by a barred potential. Such patterns (also described as "figure-of-eight") have been successfully used to infer the presence of bars in the Galaxy (Binney *et al.* 1991) and in edge-on external galaxies (e.g. García-Burillo & Guélin 1995; Kuijken & Merrifield 1995). Similar patterns have also been observed in a number of barred galaxies with moderate inclinations (e.g. M83: Handa *et al.* 1990; NGC 7479: Laine *et al.* 1999; UGC 2855: Hüttemeister *et al.* 1999).

— Figure 9 —

Figure 10 presents a model of gas orbits in a barred potential which reproduces the main features in the position-velocity diagram for NGC 5005. We calculate periodic orbits using the damped-orbit model of Wada (1994) and the formulae of Sakamoto *et al.* (1999a: Appendix B) for the case in which two inner 2:1 Lindblad resonances (ILRs) exist. We adopt

---

[5] So far, no HI observations to determine the kinematic major axis have been reported for this galaxy.

[6] Eskridge (1999) confirms the existence of a bar in near-infrared images of NGC 5005 obtained for the Ohio State University Galaxy Survey. In addition, K' snapshot images from the Palomar 60-inch telescope are consistent with a bar of length $\sim 1'$ at a position angle of $\sim 80°$.

a pattern speed for the bar which locates these resonances at radii of 1.1 and 2.1 (in dimensionless units for which corotation occurs at 10.0); this choice is motivated by considerations which follow in §4.2. The dominant orbits outside the outer ILR and inside the inner ILR are parallel to the bar and belong to the x_1 family. Between the ILRs, orbits which are perpendicular to the bar and belong to the x_2 family dominate. In the left panel of Figure 10, the x_1 orbits are horizontally elongated. At the ILRs, the position angle of the orbits differs by 45° from the bar major axis because of a damping term in the model (Wada 1994; Sanders & Huntley 1976). We note that the streamlines in a cloud-based model like this one can have sharp turns (giving rise to large velocity widths) at the leading edge of the bar (e.g. Lindblad & Lindblad 1994). Such features have been attributed by other authors (e.g. Regan *et al.* 1999) entirely to the shocks which appear in full hydrodynamic simulations. Our ability to match observations with a simpler (cloud-based) approach gives us confidence that its use here is reasonable.

— Figure 10 —

The right panel in Figure 10 shows a position-velocity cut through our model along the bar major axis. Gas particles on x_2 orbits are plotted as crosses, those on x_1 orbits at the leading edge of the bar are plotted as diamonds, and those on x_1 orbits at the trailing edge of the bar are plotted as dots. The x_1 gas at the bar's leading edge and the separate x_2 gas inside the outer ILR (i.e. the diamonds and crosses) form a "tilted X" pattern very similar to that seen in NGC 5005. Moreover, the gas on the model x_2 orbits has a maximum rotational speed much faster than the circular rotation speed for this potential (shown as a solid line). This excess arises because the tangential velocity near the pericenter of an elliptical orbit is higher than the circular velocity. Because the major axis of the bar is close to the major axis of the galaxy (i.e. the line of nodes) in NGC 5005, material on x_2 orbits will reach pericenter while moving nearly along our line of sight. The bar model thus provides a natural explanation for why the linewidth of the nuclear disk exceeds that of the galaxy's full H I line; we do not need to appeal to a large central mass.

Gas on x_1 orbits at the leading edge of the bar, producing the shallower component of the "tilted X" pattern in the model p-v diagram, appears to have a velocity *less* than circular for NGC 5005. This deficit arises (as above) because the bar and galaxy major

axes are nearly (though not exactly) parallel: streaming along the bar will occur more in the plane of the sky than along our line of sight. In the context of this model, the northwest stream seen in NGC 5005 is clearly identified as gas moving towards the nuclear disk on an x_1 orbit at the leading edge of the bar. More tentatively, we suggest that the emission at $(-20'', +100$ km s$^{-1})$ in Figure 9 may also trace the leading edge of the bar on an x_1 orbit. This feature (a possible "east stream") can be marginally distinguished inside the 3 kpc ring in the medium-resolution map of Figure 1. Little emission is seen in the regions of the p-v diagram corresponding to x_1 orbits at the trailing edge of the bar, but this is not entirely surprising. Many barred galaxies show strong concentrations of gas at the shocks which form in leading-edge dust lanes. The likely reason is that gas in a bar is directly channeled to a nuclear disk through x_1 orbits at its leading edge. After colliding with the nuclear disk near pericenter and entering onto x_2 orbits, most of the gas is unavailable to flow past the nucleus and trace the trailing edge of the bar. This distinction between the behaviors of the stellar and gaseous components is emphasized by Bureau & Athanassoula (1999) and Athanassoula & Bureau (1999) in their extensive studies of p-v diagrams for barred galaxies. Our own model confirms that p-v diagrams can sometimes tell us not only whether a bar supports two families of orbits, but also whether the gas on the x_1 orbits is at the bar's leading or trailing edge.

4.2. The origin of the 3 kpc ring

The 3 kpc ring has a nearly circular shape but clearly noncircular velocities (§3.3). Figure 5 shows position-velocity cuts along the galaxy's [isophotal] major and minor axes. The minor-axis p-v diagram clearly shows that the 3 kpc ring has some degree of noncircular (i.e. radial) motion. The gas to the south (north) of the nucleus has negative (positive) velocities with respect to the systemic velocity. The radial motion is directed inward with an amplitude of about 50 km s^{-1} on the minor axis. We consider two possible scenarios for the origin of the ring and its inward motions — that it constitutes a canonical resonance ring at the inner 4:1 Lindblad resonance, and alternately, that it is actually a pair of tightly wound spiral arms. Although we prefer the former hypothesis, the latter can not be excluded with our current data.

An inner 4:1 Lindblad resonance region occurs where $\Omega - \kappa/4$ (calculated assuming a purely ax-

isymmetric potential) is nearly equal to the pattern speed of the bar Ω_p (see reviews by Buta & Combes (1996) and Sellwood & Wilkinson (1993)); it is more widely known as the "ultraharmonic resonance" (UHR), nomenclature which we will adopt here. An "inner" ring which encircles a bar and falls inside spiral arms is often identified with the UHR (e.g. Schwarz 1984a; Buta 1986). Can the UHR ring scenario explain the inward velocities we see in NGC 5005? The pattern speed chosen to produce Figure 10 places the model's UHR at a radius of 6.3; the ratio $R_{\rm UHR}/R_{\rm OILR} \sim 3$ successfully matches the ratio between the radii of the 3 kpc ring and the nuclear disk. If the 3 kpc ring is truly a stable ring rather than a transient feature or a pair of spiral arms, its constituent clouds must follow closed orbits in the frame rotating with the bar. In this case, the velocities of material in the ring can be estimated from its shape (Buta 1986). Figure 11 shows a deprojected version of the CO(1–0) emission from NGC 5005. The 3 kpc ring is roughly circular, but is slightly elongated parallel to the bar with an axial ratio ~ 0.8, consistent with the average axial ratio of 0.82 observed for inner rings in barred galaxies (Schwarz 1984b). In a frame rotating with the bar, gas motion will be counterclockwise anywhere inside corotation, including at the putative UHR. Near the minor axis of the galaxy (i.e. on the vertical line in Figure 11), gas on an elongated orbit in the ring will therefore be on its way from apocenter to pericenter and will appear to have an inward velocity.

— Figure 11 —

A more quantitative approach is taken in Figure 12, in which line-of-sight velocities in the 3 kpc ring are plotted with respect to azimuthal angle. It is evident that circular motion alone fails to reproduce the observations, leaving velocity residuals up to ~ 100 km s^{-1}. In the UHR model, we can assume that noncircular velocities in an elongated ring will be sinusoidal with a phase delay roughly equal to the position angle of the bar. The dashed line in Figure 12 shows an elliptical-orbit model generated for this assumption which produces reasonable agreement with the observations, including the 50 km s^{-1} noncircular velocity on the galaxy's minor axis (azimuth $= \pm 90°$). Although we do not attempt parameter fitting for this model, the UHR hypothesis is qualitatively consistent with the pattern of noncircular motions in the 3 kpc ring. In this scenario, the spiral arms outside the ring need not be tightly wound, and the arm which runs

east (west) on large scales probably starts from the east (west) end of the bar.

— Figure 12 —

An alternate explanation for the 3 kpc ring is that it is not really a ring at all, but instead is a pair of tightly wound spiral arms. Streaming motions in a spiral density wave will be directed inward along the minor axis for all radii inside corotation. Numerical simulations (e.g., Roberts 1969, and Roberts & Hausman 1984) as well as observations of a number of spiral galaxies (e.g. M81, Visser 1980; M51, Vogel *et al.* 1993) show inward motions on spiral arms near the minor axis inside corotation. The velocity–azimuth angle plot in Figure 12 supports one element of the tightly wound spiral arm picture. The residual velocities from circular motion are (though somewhat scattered) sinusoidal with a period of 2π rather than $2\pi/3$, as expected for any ringlike feature inside corotation which is formed by density-wave spiral arms (Canzian 1993). A cautionary note for this scenario is the sharply different pitch angle displayed by the spiral arms at larger galactocentric radii. We would at least expect the eastern (western) spiral arm to start from the west (east) end of the bar, if the spiral arms start from the bar's ends as is usually the case in barred galaxies. However, this picture may still necessitate a zero or (unrealistically) negative pitch angle for the "arms" comprising the ring (see Figure 11). Precise determination of the galaxy's inclination and position angle (e.g. with H I mapping) and large field-of-view color index maps would both help determine whether the 3 kpc ring is a resonance ring at the UHR or is not a ring at all.

4.3. Episodic inflow to the nuclear disk

We have shown that the northwest stream is a $\sim 2 \times 10^8 \, M_\odot$ gas clump on its way from the 3 kpc ring to the nuclear disk. At an infall speed of 200 km s^{-1} and a distance of 1 kpc from the center, most of this mass should soon collide and merge with the nuclear disk; part of the stream should already be colliding with the outskirts of the disk. A crude estimate of the rate of accretion to the disk during this collision is $\dot{M} = M/(l/V) \sim 50 \, M_\odot$ yr^{-1}, where l is the size of the northwest stream and we assume that most of the stream material will merge with the nuclear disk during its first passage of pericenter (§4.1). The absence of inflowing gas along the full length of the bar means that the high accretion rate lasts for only a few Myr, and that inflow must be largely episodic

rather than continuous. The next episode after the present one may well occur as gas in the possible "east stream" moves inward. While a steady supply of tenuous gas may have escaped detection, the impending increase of the nuclear disk's mass by ~ 10 % seems likely to be more significant. As this fueling event progresses, we would expect it to produce cloud collisions, shocks, and gravitational instabilities in the nuclear disk, enhancing the star formation rate and (perhaps) the rate of inflow to the active nucleus. If the supply of gas to the nucleus is similarly episodic in other galaxies, we have a natural mechanism to regulate the intermittent triggering of nuclear starbursts, which Balzano (1983) infers have a duty cycle of ~ 5 %. A connection between kpc-scale fueling and nuclear activity is likely to be more indirect at best, since accretion luminosity can be significantly boosted by the disruption of an individual star (e.g. Eracleous *et al.* 1995) or gas cloud (e.g. Bottema & Sanders 1986).

5. Conclusions

We have observed CO(1–0) emission from the LINER galaxy NGC 5005 to study the gas dynamics in the central 6 kpc ($1'$).

1. In its central 6 kpc, NGC 5005 has three distinct molecular gas components — a roughly circular ring of radius ~ 3 kpc and gas mass $\sim 2 \times 10^9$ $M_\odot$; a central condensation with radius ~ 1 kpc and gas mass $\sim 2 \times 10^9$ $M_\odot$; and a component with size ~ 0.5 kpc and gas mass $\sim 2 \times 10^8$ $M_\odot$, located about $6''$ northwest of the nucleus. The nuclear disk shows weaker CO(1–0) emission in its innermost $100 - 200$ pc.

2. The 3 kpc ring shows noncircular velocities, with 50 km s^{-1} inward motions observed on the minor axis. The northwest stream has a very large noncircular motion; its line-of-sight velocity is ~ 150 km s^{-1} different from that of the circular galactic rotation. The nuclear disk has a linewidth ~ 30 % larger than that of the 3 kpc CO ring and of the entire galaxy's HI emission. Noncircular motions are also evident in the first moment map of the disk.

3. A stellar bar of length ~ 5 kpc may account for these gas distributions and their kinematics. The bar would run roughly east-west, placing the northwest stream and an associated straight

dust lane at its leading edge. The nuclear disk is mainly formed from x_2 orbits elongated perpendicular to the bar. The disk's large linewidth is probably due to clouds on elliptical orbits which move along our line of sight as they reach pericenter, rather than (necessarily) to a large mass concentration at the galactic center. The northwest stream lies on an x_1 orbit elongated parallel to the bar; it is falling towards the nuclear disk, with which it will ultimately collide and merge.

4. The 3 kpc ring may form at the ultraharmonic resonance of the bar or (rather improbably) constitute a pair of spiral arms which originate at its ends. Noncircular motion would be explained in these scenarios by orbital motions in an elongated ring and by spiral-arm streaming, respectively.

5. The supply of gas to the nuclear disk is episodic rather than continuous. Gas from the outer galaxy will accumulate in the 3 kpc ring and occasionally fall to the nuclear disk, as in the case of the northwest stream, due to the action of the bar. The present fueling event will ultimately increase the mass of the nuclear disk (by about 10 %) and impact star formation there within several Myr. A subsequent fueling event may occur if gas in the possible "east stream" is truly flowing along the bar. Such episodic supply of gas may be responsible for triggering intermittent nuclear starbursts in other disk galaxies.

A future paper (Baker *et al.* 1999) will present further analysis of the nuclear disk and its relation to fueling of the LINER, based on $1''$ resolution maps of multiple molecular lines.

REFERENCES

Athanassoula, E. & Bureau, M. 1999, ApJ, 522, 699

Baker, A. J., Sakamoto, K., & Scoville, N. Z. 1999, in preparation

Balzano, V. A. 1983, ApJ, 268, 602

Binney, J., Gerhard, O. E., Stark, A. A., Bally, J., & Uchida, K. I. 1991, MNRAS, 252, 210

Bottema, R. & Sanders, R. H. 1986, A&A, 158, 297

Braine, J., Combes, F., Casoli, F., Dupraz, C., Gérin, M., Klein, U., Wielebinski, R., & Brouillet, N. 1993, A&AS, 97, 887

Bureau, M. & Athanassoula, E. 1999, ApJ, 522, 686

Buta, R. 1986, ApJS, 61, 631

Buta, R. & Combes, F. 1996, *Fund. Cosmic Physics*, 17, 95

Canzian, B. 1993, ApJ, 414, 487

Condon, J. J., Helou, G., Sanders, D. B., Soifer, B. T. 1990, ApJS, 73, 359

de Vaucouleurs, G., de Vaucouleurs, A., Corwin, H. G., Buta, R. J., Paturel, G., & Fouqué, P. 1991, "Third Reference Catalogue of Bright Galaxies" (New York: Springer-Verlag)

Eracleous, M., Livio, M., & Binette, L. 1995, ApJ, 445, L1

Eskridge, P. B. 1999, private communication

Filippenko, A. V., & Sargent, W. L. 1985, ApJS, 57, 503

García-Burillo, S., & Guélin, M. 1995, A&A, 299, 657

Goodrich, R. W., & Keel, W. C. 1986, ApJ, 305, 148

Handa, T., Nakai, N., Sofue, Y., Hayashi, M., & Fujimoto, M. 1990, PASJ, 42, 1

Ho, L. C., Filippenko, A. V., & Sargent, W. L. W. 1997, ApJS, 112, 391

Hüttemeister, S., Aalto, S., & Wall, W.F. 1999, A&A, 346, 45

Keel, W. C. 1983, ApJS, 52, 229

Kuijken, K. & Merrifield, M. R. 1995, ApJ, 443, L13

Laine, S., Kenney, J. D. P., Yun, M. S., & Gottesman, S. T. 1999, ApJ, 511, 709

Lindblad, P. O., & Lindblad, P. A. B. 1994, "Physics of the Gaseous and Stellar Disks of the Galaxy", I. R. King ed., (ASP Conf. Ser. 66), 29

Regan, M. W., Sheth, K., & Vogel, S. N. 1999, ApJ, in press (astro-ph/9908121)

Risaliti, G., Maiolino, R., & Salvati, M. 1999, ApJ, 522, 157

Roberts, W. W. 1969, ApJ, 158, 123

Roberts, W. W., & Hausman 1984, ApJ, 277, 744

Sakamoto, K., Okumura, S., Ishizuki, S., & Scoville, N. Z. 1999a, ApJS, 124 (Oct. issue), in press (NRO report No. 499. available from http://www.nro.nao.ac.jp/~eiko/nroreport/)

Sakamoto, K., Okumura, S., Ishizuki, S., & Scoville, N. Z. 1999b, ApJ, 525, (10 Nov. issue), in press (astro/ph-9906454)

Sanders, R. H., & Huntley, J. M. 1976, ApJ, 209, 53

Schwarz, M. P. 1984a, MNRAS, 209, 93

Schwarz, M. P. 1984b, A&A, 133, 222

Scoville, N. Z., Yun, M. S., Clements, D. P., Sanders, D. B., & Walker, W. H. 1987, ApJS, 63, 821

Scoville, N. Z., Carlstrom, J. E., Chandler, C. J., Phillips, J. A., Scott, S. L., Tilanus, R. P. J., & Wang, Z. 1993, PASP, 105, 1482

Sellwood, J. A., & Wilkinson, A. 1993, *Rep. Prog. Phys.*, 56 173, §7

Solomon, P. M., Rivilo, A. R., Barrett, J., & Yahil, A. 1987, ApJ, 319, 730

Strong, A. W., Bloemen, J. B. G. M., Dame, T. M., Greiner, I. A., Hermsen, W., Lebrun, F., Nyman, L.-A., Pollock, A. M. T., & Thaddeus, P. 1988, A&A, 207, 1

Tully, R. B. 1988, "Nearby Galaxies Catalog" (Cambridge: Cambridge Univ. Press)

van der Hulst, J. M., Crane, P. C., & Keel, W. C. 1981, AJ, 86, 1175

Vila, M. B., Pedlar, A., Davies, R. D., Hummel, E., & Axon, D. J. 1990, MNRAS, 242, 379

Visser, H. C. D. 1980, A&A, 88, 159

Vogel, S. N., Rand, R. J., Gruendl, R. A., & Teuben, P. J. 1993, PASP, 105, 666

Wada, K. 1994, PASJ, 46, 165

White, R. L., Becker, R. H., Helfand, D. J., & Gregg, M. D. 1997 ApJ, 475, 479

Young, J. S., Xie, S., Tacconi, L., Knezek, P., Viscuso, P., Tacconi-Garman, L., Scoville, N., Schneider, S., Schloerb, F. P., Lord, S., Lesser, A., Kenney, J., Huang, Y.-L., Devereux, N., Claussen, M., Case, J., Carpenter, J., Berry, M., & Allen, L. 1995, ApJS, 98, 219

Fig. 1.— CO(1–0) zeroth and first moment maps of NGC 5005. Synthesized beams are shown in the lower left corners; large crosses mark the dynamical center at $\alpha_{1950} = 13^{\rm h}08^{\rm m}37\overset{\rm s}{.}67$ and $\delta_{1950} = +37°19'28\overset{''}{.}34$. (Top row) Low-resolution ($4''$) maps. The ellipse is centered on the dynamical center, and has major and minor axes of $60''$ and $60'' \cos 62°$ with a position angle of $65°$, which corresponds to a circle in the galactic plane after deprojection. (Middle row) Medium-resolution ($2\overset{''}{.}7$) maps. (Bottom row) High-resolution ($1\overset{''}{.}5$) maps of the nuclear gas disk. The small crosses mark the mean position of the radio continuum nucleus.

Fig. 2.— Low-resolution channel maps of CO(1–0) emission from NGC 5005. Each panel is labeled with the LSR velocity in km s^{-1}. The synthesized beam is shown in the lower left corner of the first panel. The ellipse is identical to that shown in Figure 1.

Fig. 3.— Optical image of NGC 5005 ($\lambda = 550$ nm). North is to the top and east is to the left.

Fig. 4.— The low-resolution CO(1–0) map overlaid on the HST V-band image of NGC 5005. Dark dust lanes and molecular gas correlate well.

Fig. 5.— Position–velocity cuts along the major and minor axes of the galaxy (p.a. $65°$ and $155°$, respectively), made from the medium-resolution data. Position is measured from the dynamical center, and velocity is relative to 932.8 km s^{-1}.

Fig. 6.— The central $14'' \times 14''$ of NGC 5005. The high-resolution CO(1–0) map is overlaid on the HST V-band image. The cross marks the radio nucleus.

Fig. 7.— Medium-resolution CO(1–0) channel maps for channels containing emission from the northwest stream, the centroid of which is shown as a cross. Each panel is labeled with the LSR velocity in km s^{-1}. The synthesized beam is shown in the lower left corner of the first panel. The ellipse is identical to that shown in Figure 1.

Fig. 8.— Schematic view of the gas distributions in NGC 5005. The 3 kpc ring, the nuclear molecular disk, and the northwest stream are seen in CO, as is a possible "east stream." A dust lane between the nuclear disk and the 3 kpc ring (coincident with the northwest stream) and the outer spiral arms are suggested from dark lanes in optical images. A bar or oval distortion shown as a dashed ellipse is inferred from the gas distribution and kinematics. The major axis of the galaxy has p.a. $65°$; the northwest side of the galaxy is near to us; and the sense of rotation is counterclockwise.

Fig. 9.— Position–velocity cut along the bar (p.a. $80°$) through the dynamical center, made from the low-resolution data. The cut is $5''$ wide and contains the northwest stream at about ($+5''$, $+100$ km s^{-1}) and the possible "east stream" at about ($-20''$, $+100$ km s^{-1}). The velocity zero-point is 937.9 km s^{-1}.

Fig. 10.— (Left) Model orbits in a barred potential, in a frame rotating with the bar. The bar runs horizontally (along the dashed line) and rotates counterclockwise. The potential is $\Phi(r, \theta) = -(1 + \varepsilon \cos 2\theta) \log(1 + r^2)/2$, where (r, θ) are polar coordinates rotating with the bar and the strength of the bar is $\varepsilon = 0.04$. The pattern speed of the bar is 0.1, which places the inner and outer ILR, UHR, and corotation radii at 1.1, 2.1, 6.3, and 10, respectively. The orbits are calculated using a damped orbit model (Wada 1994). Horizontally elongated orbits are x_1 orbits, while vertically elongated ones are x_2 orbits. (Right) Position–velocity cut (of full spatial width 8) through the model galaxy at left, along the bar major axis. The solid line shows the circular velocity curve. Gas particles on different orbits are plotted with different symbols: crosses are on x_2 orbits, diamonds are on x_1 orbits at the leading edge of the bar, and dots are on x_1 orbits at the trailing edge of the bar. Gas on x_2 orbits and on x_1 orbits at the leading edge of the bar (i.e. crosses and diamonds) form a "tilted X" pattern like that seen in Figure 9 for NGC 5005. Velocities have been corrected for inclination, assuming that the line of nodes and the bar major axis differ by $30°$ in the plane of the galaxy.

Fig. 11.— Face-on view of NGC 5005, made from the low-resolution map. Deprojection assumed $i = 62°$ and P.A. $= 65°$. Primary-beam correction has been applied. In this figure, the line of nodes is horizontal, the reference circle has a $30''$ radius, and the line at p.a. $\approx -45°$ shows the approximate position angle of the bar (east-west in the sky plane). The approaching side of the galaxy is to the right, and the near side is at top. Gas rotates counterclockwise.

Fig. 12.— Velocities on the 3 kpc ring are plotted as a function of azimuthal angle θ in the galactic plane,

where θ is measured counterclockwise from the receding major axis (p.a. $= 65°$). Data points (asterisks) are mean line-of-sight velocities for the ring ($R = 25'' - 35''$) with $\pm 1\sigma$ standard deviations, measured from the low-resolution CO data. The solid curve shows velocities expected for circular rotation with azimuthal velocity $V_{\mathrm{az}} = 295$ km s^{-1} in the galactic plane ($V_{\mathrm{sys}} = 952$ km s^{-1}). The dotted curve shows the expectation for an oval orbit with $V_{\mathrm{rad}} = -60 \sin 2(\theta - 30°)$ and $V_{\mathrm{az}} = 295 - 30 \cos 2(\theta - 30°)$. At bottom are the residual velocities for each model. The 30° phase offset corresponds to the difference between line of nodes and bar major axis which was used to correct Figure 10 for inclination.

TABLE 1

PARAMETERS OF NGC 5005

Parameter	Value	Ref.
Hubble type	SAB(rs)bc	(1)
Distance [Mpc]	21.3	(2)
P.A. (isophotal) [°]	65	(1)
inclination (isophotal) [°]	62	(1)
V_{sys} [km s^{-1}][a]	952	(1)
B_T^0 [mag]	10.19	(1)
$S_{\mathrm{CO(1-0)}}(45'')$ [Jy km s^{-1}]	697 ± 90	(3)
$S_{\mathrm{CO(1-0)}}(23'')$ [Jy km s^{-1}]	435 ± 31	(4)

NOTE.— References are (1) de Vaucouleurs *et al.* (1991); (2) Tully *et al.* (1988); (3) Young *et al.* (1995), 45″ (FHWM) beam centered at $\alpha_{1950} = 13^{\mathrm{h}}08^{\mathrm{m}}37\overset{s}{.}6$ and $\delta_{1950} = +37°19'25''$; (4) Braine *et al.* (1993), 23″ (FWHM) beam centered at $\alpha_{1950} = 13^{\mathrm{h}}08^{\mathrm{m}}37\overset{s}{.}7$ and $\delta_{1950} = +37°19'28\overset{''}{.}5$.

[a]HI velocity, converted to the LSR velocity in the radio convention.

TABLE 2

PARAMETERS OF CO(1–0) MAPS

Resolution (1)	Configs & Weighting (2)	Beam (3) ″	″	°	V_{res} (4) km s^{-1}	σ (5) mJy bm^{-1}	mK	$f_{45''}$ (6) %	$f_{23''}$ (7) %
Low	L+H; NA	4.57	3.46	−21.25	31.1	9.9	58	75	92
Medium	L+H+U; UN, robust 2.0	2.88	2.44	−18.88	10.4	13.8	181	73	94
High	L+H+U; UN, robust -0.5	1.55	1.42	−89.95	20.7	16.8	705	47	75

NOTE.— Col. (2): L,H,U are the observing configurations. UN = uniform weighting, NA = natural weighting. Col. (3): Full width at half maximum along the major and minor axes of the beam, and position angle of the major axis. Col. (4): Velocity width of each channel map. Col. (5): 1σ noise level expressed in intensity and brightness temperature. Col. (6): Fraction of flux recovered in the data cube, out of total seen by the FCRAO 14 m telescope in a 45″ FWHM beam (Young *et al.* 1995). Col. (7): Fraction of flux recovered in the data cube, out of total seen by the IRAM 30 m telescope in a 23″ FWHM beam (Braine *et al.* 1993).

TABLE 3

POSITION OF THE NUCLEUS

#	R.A. (B1950)			Dec. (B1950)			Resolution	λ_{obs}	Ref.
	h	m	s	°	′	″	″	cm	
1	13	08	37.68	+37	19	28.77	1	6	(a)
2	13	08	37.67	+37	19	28.4	1.5	20	(b)
3	13	08	37.69	+37	19	28.6	1.0	6,20	(c)
4	13	08	37.651	+37	19	28.80	5	20	(d)
5	13	08	37.673	+37	19	28.64	$\cdots$	$\cdots$	(e)
6	13	08	37.67	+37	19	28.34	1.5	0.3	(f)

NOTE.—Sources are (a) van der Hulst *et al.* (1981); (b) Condon *et al.* (1990); (c) mean of 6 and 20 cm positions in Vila *et al.* (1990); (d) VLA/FIRST survey (White *et al.* 1997), converted from J2000 to B1950; (e) arithmetic mean of 1,2,3, and 4; (f) this paper: dynamical center determined from the high-resolution CO(1–0) data.

TABLE 4

KINEMATIC PARAMETERS OF THE NUCLEAR DISK

Parameter	Value
Dynamical center α_{1950}	$13^{\mathrm{h}}08^{\mathrm{m}}37\overset{\mathrm{s}}{.}67$
δ_{1950}	$+37°19'28\overset{''}{.}34$
P.A. [°]	70
inclination [°]	53
V_{sys} [km s^{-1}]	928[a]
Velocity range [km s^{-1}]	565 – 1301[b]
ΔV [km s^{-1}]	736[b]

NOTE.—All values except the velocity range and the linewidth are determined from a fit to the high-resolution first moment map in Figure 1. The northwest stream is excluded from the fit. For the remainder of our analysis, we adopt the very similar isophotal position angle and inclination in Table 1.

[a]LSR velocity defined in the radio convention.

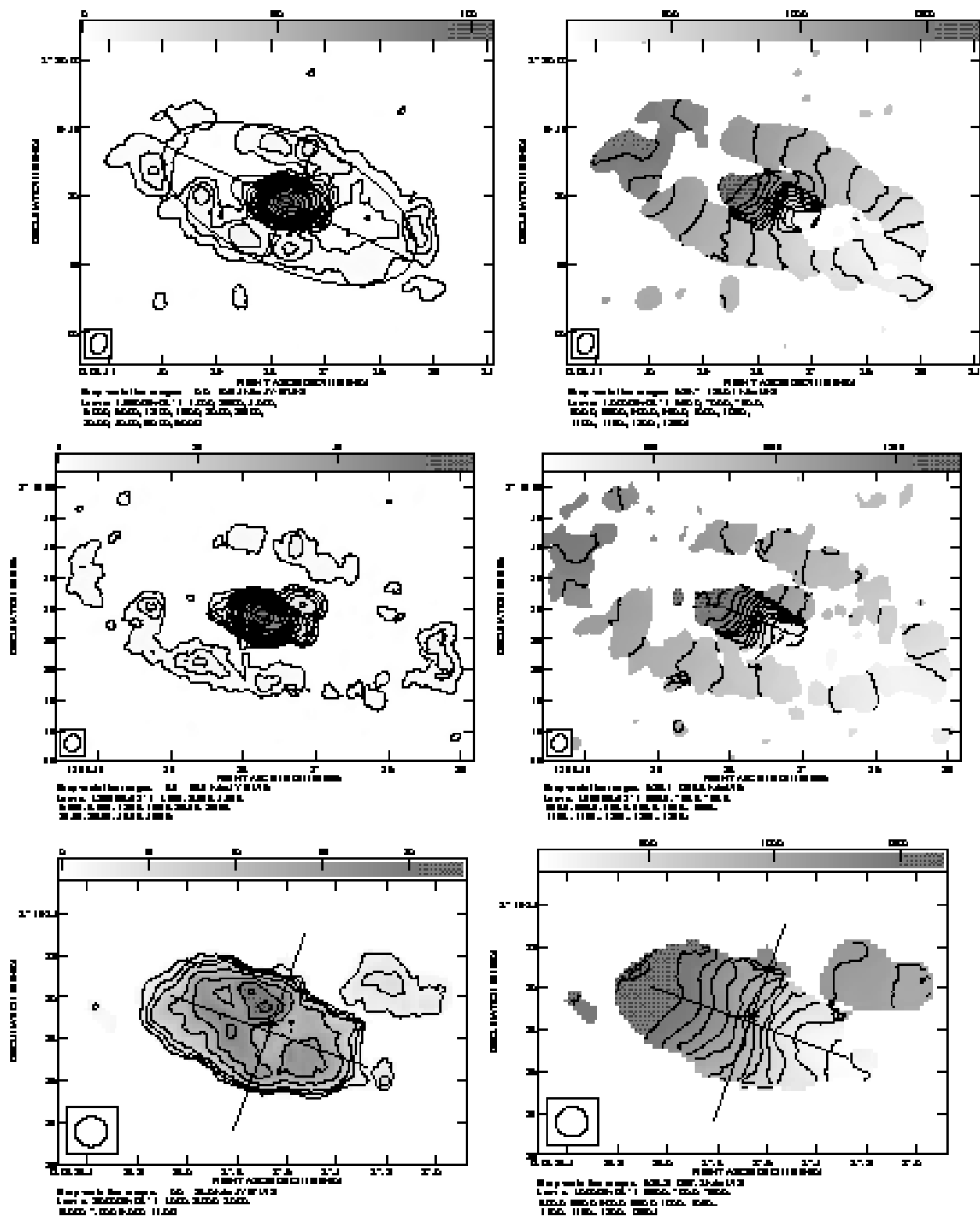[b]Includes channels with emission at the 3σ level in the medium-resolution data cube.

15

TABLE 5

GAS AND DYNAMICAL MASSES

Radius[a]		M_{dyn}[b]	M_{gas}[c]	$M_{\mathrm{gas}}/M_{\mathrm{dyn}}$
$''$	kpc	$10^{10}\ M_\odot$	$10^{9}\ M_\odot$	%
5	0.5	2.1	1.4	7
30	3.1	6.3	4.0	6

[a]Radius in the galactic plane.

[b]Rotation velocities are measured from the major axis position-velocity diagram in Figure 5. The dynamical mass in the central $5''$ is probably overestimated because of noncircular motion (see §4.1).

[c]CO fluxes are measured from the medium-resolution data for $R \leq 5''$ and from the low-resolution data for $R \leq 30''$.

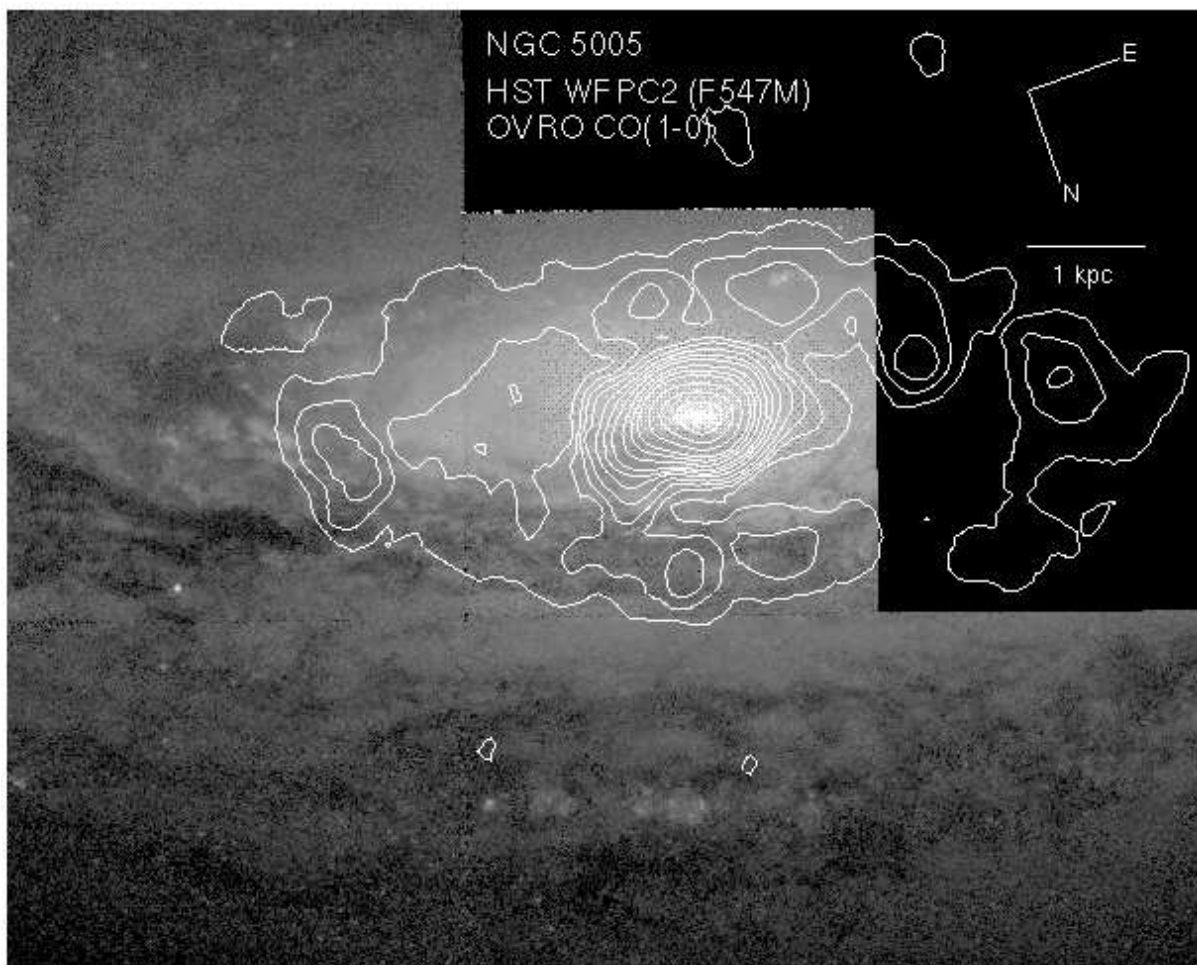Fig. 1.— Quality of this figure was lowered for astro-ph. A PS preprint with the full-resolution figures is avaiable from http://www.ovro.caltech.edu/mm/science/science.html .

Fig. 2.— Quality of this figure was lowered for astro-ph. A PS preprint with the full-resolution figures is avaiable from http://www.ovro.caltech.edu/mm/science/science.html .
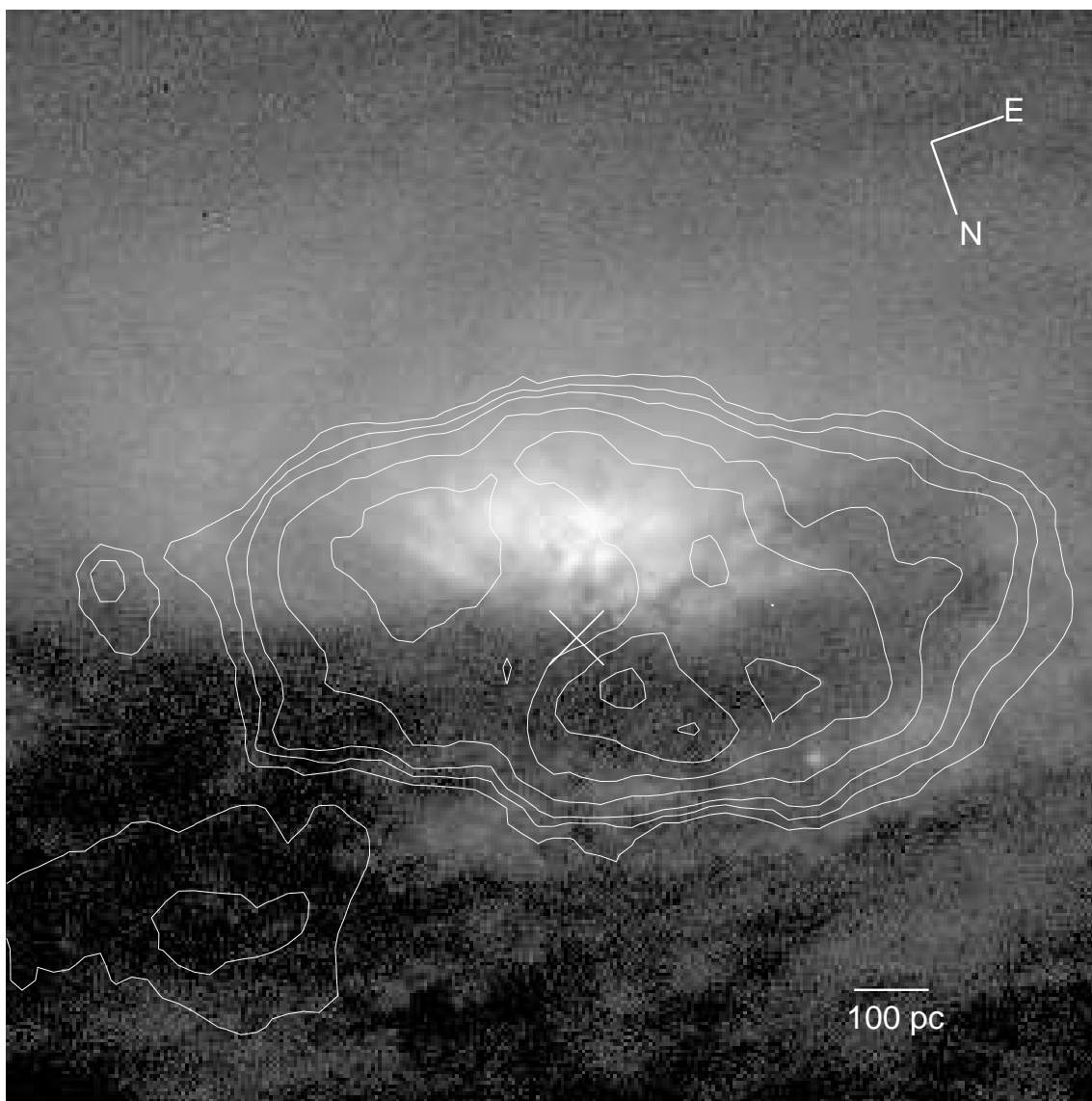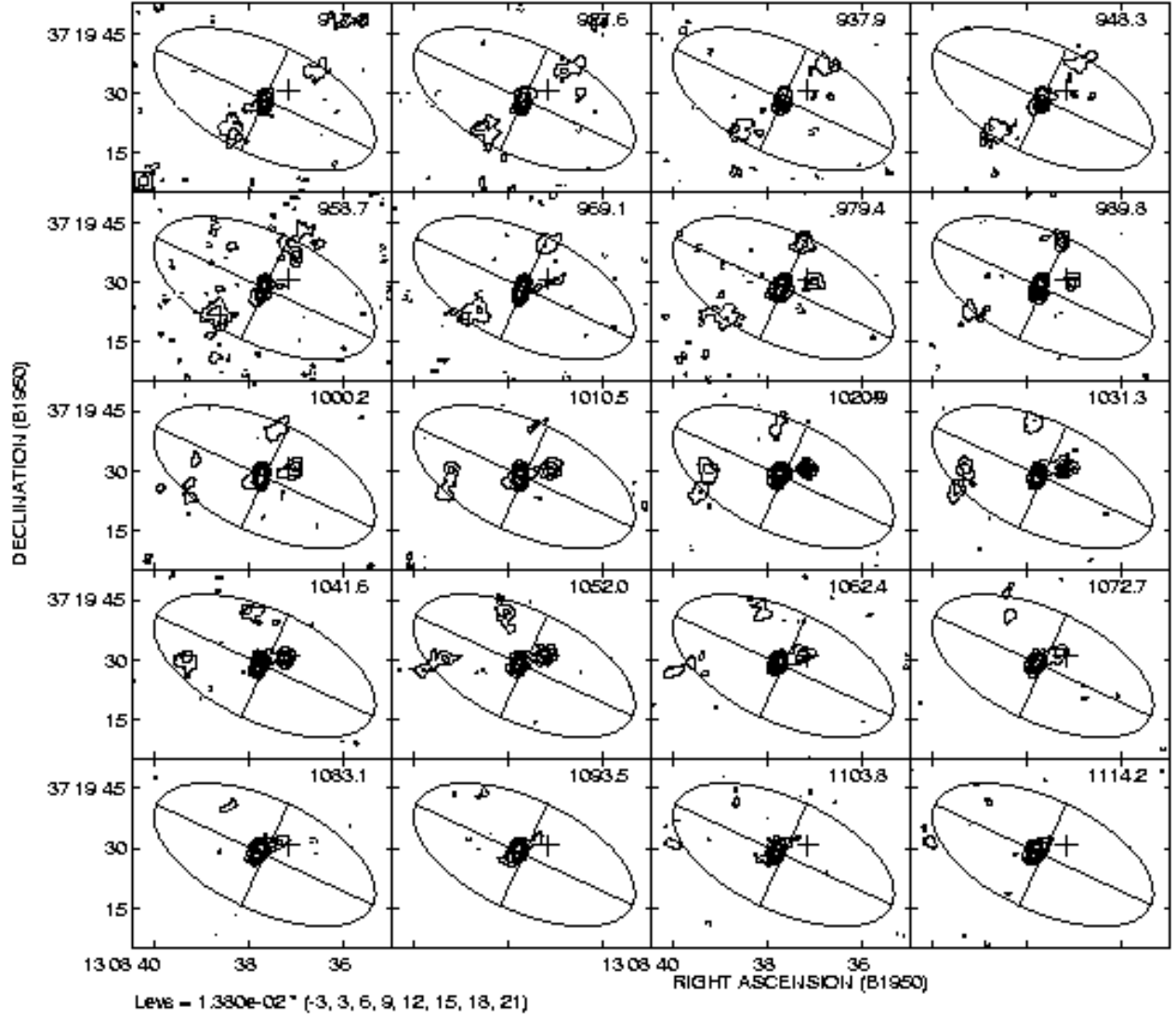
Fig. 3.— Quality of this figure was lowered for astro-ph. A PS preprint with the full-resolution figures is avaiable from http://www.ovro.caltech.edu/mm/science/science.html .

Fig. 4.— Quality of this figure was lowered for astro-ph. A PS preprint with the full-resolution figures is avaiable from `http://www.ovro.caltech.edu/mm/science/science.html`.

Fig. 5.— Quality of this figure was lowered for astro-ph. A PS preprint with the full-resolution figures is avaiable from `http://www.ovro.caltech.edu/mm/science/science.html` .

Fig. 6.—

Fig. 7.— Quality of this figure was lowered for astro-ph. A PS preprint with the full-resolution figures is avaiable from http://www.ovro.caltech.edu/mm/science/science.html .
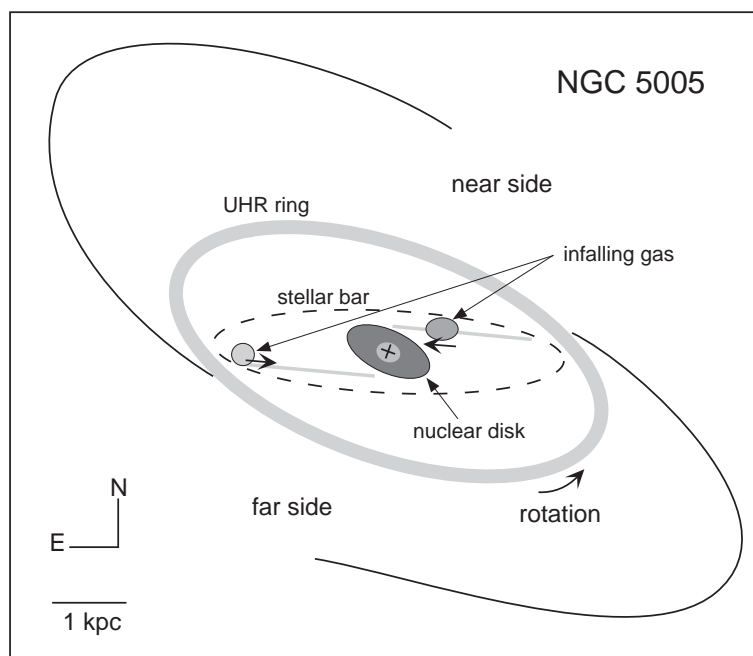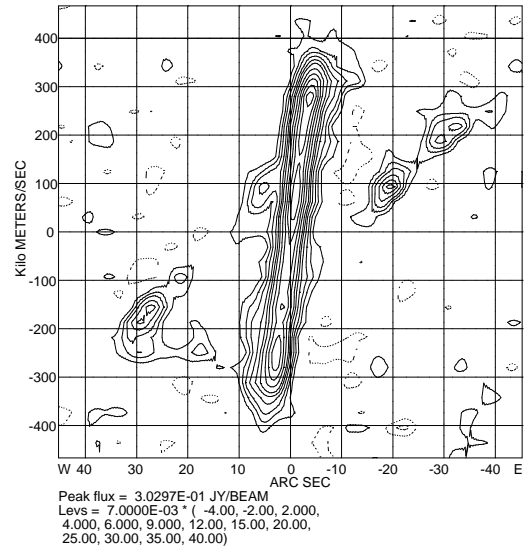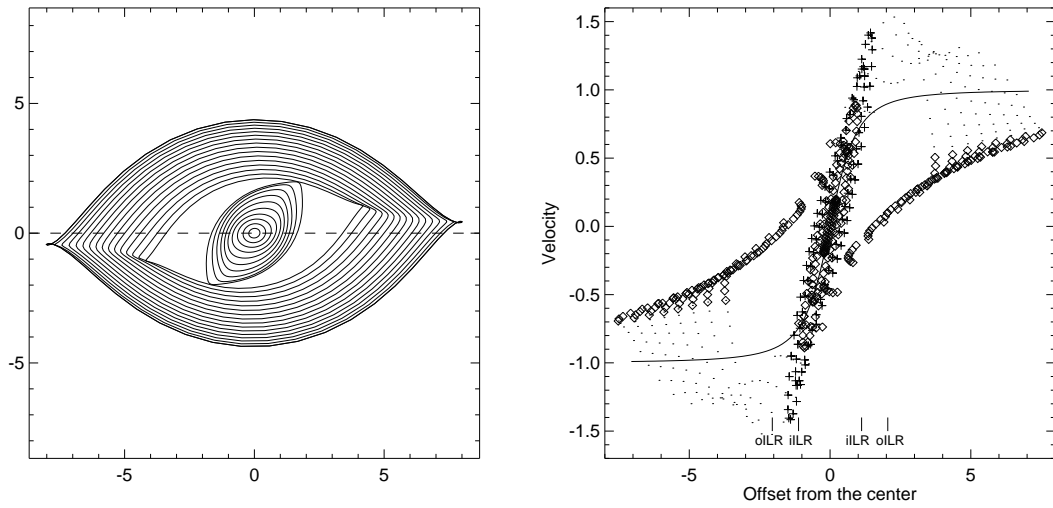
NGC 5005

near side

UHR ring

infalling gas

stellar bar

nuclear disk

N

E

far side

rotation

1 kpc

Fig. 8.—

Peak flux = 3.0297E-01 JY/BEAM
Levs = 7.0000E-03 * (-4.00, -2.00, 2.000,
4.000, 6.000, 9.000, 12.00, 15.00, 20.00,
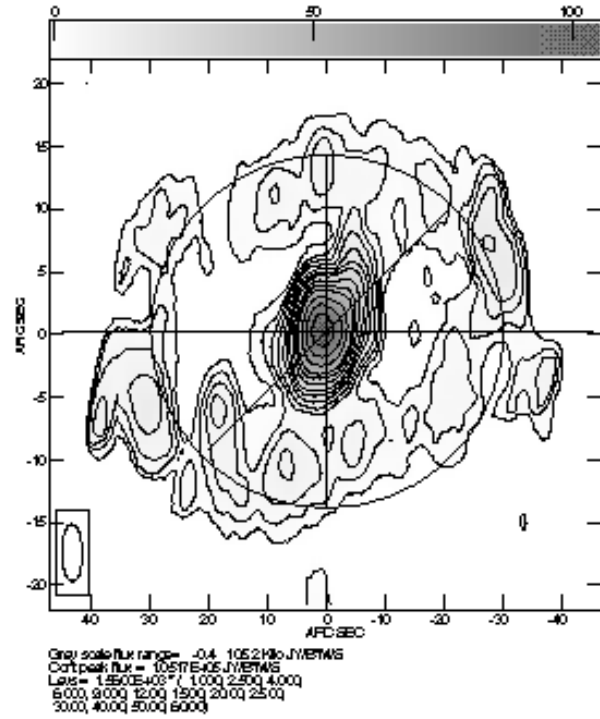25.00, 30.00, 35.00, 40.00)

Fig. 9.—

Fig. 10.—

25

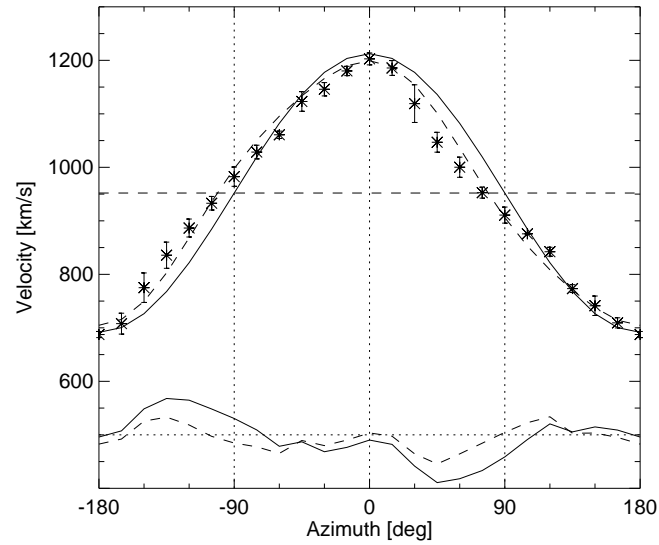Fig. 11.— Quality of this figure was lowered for astro-ph. A PS preprint with the full-resolution figures is avaiable from `http://www.ovro.caltech.edu/mm/science/science.html` .

Fig. 12.—